P5.6

MESOSCALE BASIN FLOWS IN THE NOCTURNAL BOUNDARY LAYER: MODELING AND VERIFICATION

A. Mira[(1)]*, J. Cuxart[(1)], A. Luque[(1)] and J.A. Guijarro[(2)]

Universitat de les Illes Balears[(1)] and Instituto Nacional de Meteorología[(2)] , Spain

1 INTRODUCTION

The study of the atmospheric boundary layer in complex terrain is difficult. The orographical patterns generate circulations that usually follow the diurnal cycle when the synoptic winds are weak. In the nighttime, katabatic flows generate on the slopes of the mountains, that converge to the valleys and then to the basins. There are, usually, few available observations and a first approach to the understanding of the nocturnal dynamics in a basin can be through mesoscale modelling. An example of the use of this tool to the study of a slope flow can be found in Martinez et al. (2006, this conference).

In this work we address the problem of the verification of a nocturnal clear-air mesoscale simulation. In the nighttime, the circulations vary much in relatively short distances, since strong katabatic jets might be close to cold pools in basins or warm mountain tops. A mesoscale simulation normally is able to produce qualitatively a behaviour like just described, but the computed fields might be not close enough to the reality due to misplacements of the main structures, or over- or underestimations of the values of the wind, temperature and moisture. The low number of stations makes difficult to check if the model is functioning adequately. An attempt is made here to extend the verification of such a simulation making use of the available satellite imagery, allowing to re-interpret a posteriori the main conclusions of the study.

A mesoscale simulation of a spring nighttime (April 29 2005) for the Majorca Island (Western Mediterranean Sea, 200 km offshore of the Iberian Peninsula) is made. The horizontal resolution is of 1 km and the vertical resolution is 3m close to the ground, softly decreasing with height. A high pressure system is over the area, the pressure gradients are slack, the humidity is low, clear skies and there is preminence of local winds on the island. Only ten automatic weather stations are distributed along the island (Figure 1), which has a characteristic size of about 100 km. The run is made with the Meso-NH model (Lafore et al., 1998) in the supercomputer of the European Center for Medium-range Weather Forecasts.

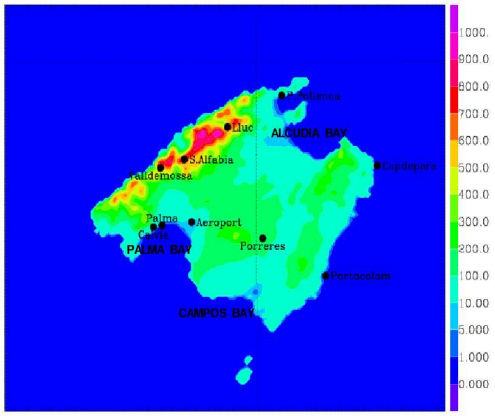

Figure 1: Orography of the Mallorca island (in meters) and location of the weather stations in the Meso-NH inner domain

Most of the studies on katabatic flows with mesoscale models have been made for high latitudes (see Bromwich et al., 2001 and references therein) and more recently on mid-latitudes (Soriano et al. 2005). The satellite imagery has been used as a complementary tool to understand the process since Bromwich (1989), that used a warm signature on winter thermal infrared (TIR)

*Corresponding author address: Antoni Mira Navarro, Grup de Meteorologia, Dpt. Física, Universitat de les Illes Balears, Ctra. Valldemossa, km 7,5, 07122-Palma de Mallorca, Spain; email: toni.mira@uib.es

NOAA images in order to study katabatic winds. In this work we try to develop objective methods to proceed to the verification of the model outputs, taking as the observed field the surface radiative temperature estimated from available satellites (NOAA and Meteosat Second Generation - MSG-). Estimation of surface temperature from MSG satellite images (Dash, 2002) is not still fully exploited, but some cloudiness studies have been performed which have demonstrated the high utility of these images (Chaboureau et al, 2000; for instance).

There are many types of methods used in verification, depending on the nature of forecast, the space-time domain, and the specificity of forecast. For the present study, the interest will be focused on methods for forecast of continuous variables. In that case, a large variety of statistical parameters such as mean error, correlation coefficient and bias can be computed, and all of them can be used to determine the forecast quality [Bromwich et al., 2001]. In addition, probability density functions [as in Jiménez and Cuxart, 2005] are computed from the model and the satellite images to compare how the surface temperature is distributed in both cases.

The methodology has several difficulties. The NOAA satellite images (resolution: 1 km at nadir) are available only once or twice per night, and the MSG (one every 15 minutes) have a coarser spatial resolution (3 km at nadir). On the other hand, point to point verification is conditioned by the location of the AWS. For the case of the Majorca island, one can differenciate the areas as coast, mountain and flat. When data from AWS located at the coast line or on the mountains are compared to model outputs, the interpolations performed by the model can modify significately the orography or the coastline of these regions, and the model will have difficulties on properly capturing the observed values at the AWS, as in Prabha et al (1999). Moreover, circulations comming from all scales are measured by the AWS, but the model is not able to simulate the smallest scale topographic fluxes.

The observational data and the characteristics of the simulation are given in the next two subsections, whereas the the verification process and the re-interpretation of the simulation are made in sections 4 and 5, leading finally to the summary and conclusions.

2 OBSERVATIONAL DATA

a. AWS data

A total of 10 AWS from the Spanish Met Office are distributed all over the isle of Majorca. There measurements of 10m wind direction and velocity, 2m temperature, humidity, precipitation and atmospheric pressure are taken each 10 minutes.

The location of the AWS is very irregular (Fig.1). Half the stations are placed near the coast, and 3 of them are placed at the northen mountain range. On Table 1 modeled and measured heights of AWS is presented, showing that in some places there exists a high difference between real and modeled orography, as for example in Serra Alfàbia or Valldemossa stations, all two located at complex orography zones. Such differences have to be considered also in other stations where its values are not so high, as in the case of Lluc station, which is placed in a small valley at the northern mountain range. There the modeled orography is smoothed and thus the little valley does not exist in the model.

b. NOAA imaginery

The AVHRR/3 scanning radiometer of NOAA-16 satellite images used in the present study uses 6 detectors that collect bands of different radiation wavelengths. Although the AVHRR/3 has sis channels, only five are transmitted to the ground. Channels 1 (0.58-0.68μm) and 2 (0.73-1.00μm) provide data in the visible-near infrared region, while channels 3 (3.55-3.93μm), 4 (10.30-11.30μm) and 5 (11.50-12.50μm) provide data in the thermal infrared region. Land surface temperature (LST) can be obtained from these data by using an split-window equation which takes account of the absortion and emission of the Earth's atmosphere and the nonblackness of natural emitting surfaces. In general, LST split-window algorithms take the form of linear combinations of the satellite brightness temperature. However, a large variety of split-window equations for the retrieval of LST can be found (e.g. Coll et al, 1994; Sobrino et al, 1996), depending on the expressions and values proposed for the algorithm coefficients.

Two NOAA images were selected, one of them at 21:25 UTC on the 28th and the other one at 03:28 UTC on the 29th. Both images had Ma-

jorca at less than 30 degrees from nadir. The pre-processing of NOAA satellite data consists in applying radiometric, geometric and atmospheric corrections. The radiometric correction (Di and Rundquist, 1994) converts digital numbers reflectances at the top of atmosphere (TOA) (in optical bands) and brightness temperatures (in thermal bands) using the coefficients included in the AVHRR data files. After the calibration, the images are geo-referenced to the Lambert Conformal Conic map projection system (Datum: European 1979 mean). They are rectified and resampled using 9 ground control points (GCPs) selected from the coastline dataset and the nearest neighbour algorithm. The atmospheric correction estimates the reflectance at the top of the canopy (TOC) from TOA reflectance by removing the atmospheric water vapor absortion (estimated from the column above Majorca). Finally, a daytime image is used to obtain the soil emissivity, which is necessary to decouple the dependence of the surface radiative temperature with the soil type. The split-window algorithm used is the one developed by Coll et al. (1997), and takes the form

$$T = T_4 + [1.34 + 0.39(T_4 - T_5)](T_4 - T_5) + 0.56 + \alpha(1-\epsilon) - \beta\Delta\epsilon$$

where T is the actual surface radiative temperature (not valid over the sea), T_4 and T_5 are the brightness temperatures in channels 4 and 5, ϵ is the soil emissivity, and $\Delta\epsilon = \epsilon_4 - \epsilon_5$ is the emissivity difference on these channels.

c. MSG-1 imaginery

MSG's Spinning Enhanced Visible and Infrared Imager (SEVIRI) provides measurements of the Earth-disc every 15 minutes in 12 spectral channels; from these, channel 9 ($10.8\mu m$) gives the best approximation to the actual LST value, since the transmission around $11\mu m$ is less affected by H_2O than for the rest of the spectral interval (Prata et al, 1995), that is, between 8 and $13\mu m$. These images are used to check the temporal evolution of the surface temperature, and without an available adapted equation for SEVIRI similar to the one described for AVHRR channels, we decided to use the channel 9 temperature without any additional correction than those included in the Level 1.5 format of the adquired images, which are corrected for radiometric and geometric non-linearity, before onward distribution to the user (*http://www.eumetsat.int*). It is important to notice that channel 9 temperature is smaller than the real one due to the atmospheric attenuation, typically between 1 and 2 degrees (Coll et at, 1994). Therefore, the MSG images indicate the temporal evolution of TSRAD, but not its absolute value. For the present work, 28 MSG images were used to construct time series of TSRAD and compare them to the model outputs and AWS data, from 1830 UTC 28 April 2005 until 0900 UTC 29 April 2005.

3 DESCRIPTION OF THE SIMULATION

Meso-NH [Lafore et al., 1998] is the non-hydrostatic mesoscale atmospheric model of the French research community. The model is intended to be applicable to all scales ranging from large (synoptic) scales to small (large eddy) scales.

The simulation is run with two domains in 1-way nesting configuration. The outer domain (the Balearics) consists of 50 grid points in the north-south direction and 75 points in the east-west direction, and the inner domain (isle of Majorca) consists of 125 grid points in the north-south direction and 150 grid points in the east-west direction (Fig.1). Their horizontal resolution is respectively 5 km and 1 km. The resolution of the inner domain is the maximum one, due to the limitation in the soil scheme database. Moreover, increasing such resolution would complicate the problem, since turbulence scheme is not well defined for hundred metres resolutions. Regarding the vertical resolution, since mountain winds develop in a shallow layer near the surface, a high resolution is also needed to accurately simulate them. A total of 85 vertical levels are used, of which 25 are located within the lowest 100 m with a spacing of 3m near the ground. Analysis from the ARPEGE (Action de Recherche Petite Echelle Grande Echelle) French model are used as initial conditions and to force the model at its boundaries. The model is initialized with the 12 UTC ARPEGE analyses on 28 April 2005 and run for 6 hours with just the 5-km resolution domain. After that, the simulation is reinitialized with the 1800 UTC ARPEGE analyses and run until 09 UTC on 29 April 2005 with both 1-km and 5-km nested domains.

The simulated period (28-29 April 2005) is characterized by weak synoptic pressure gradients

and light winds from east. During the day, the model shows how winds flow from the sea into inland and the higher temperatures occur at the lower lying areas, but as the night advances the behavior is inverted: winds flow towards the sea and the cooling is very intense at the lower lying areas of the island and at the small valleys (up to 10 K). Light winds (about 1 m/s) are observed in most of points of inland until the katabatic winds become important (0000 UTC), although the model tends to overestimate them. From then on, descendant currents coming from several parts of the island are established: on one hand, those generated at the northern mountain range, which flow towards the two large basins (Palma and Alcúdia) and, on the other hand, those generated at the eastern mountain range flowing towards the sea against synoptic wind, forcing it to surround the island. According to simulated and observed 2m-temperatures, minimum temperatures are reached between 0400 UTC and 0500 UTC. Modeled minimum temperature areas are located at points where wind remains weak during nighttime, corresponding in most of cases to the lowest areas of the island.

4 PROCESS OF VERIFICATION

4.1 Surface radiative temperature

a. Verification of the Meso-NH TSRAD with NOAA imaginery

The TSRAD processed satellite images are compared to the corresponding model outputs at 21:30 UTC and 03:30 UTC respectively. The differences are larger at 21:25 UTC since the extension of the cold areas is larger in the model than in the satellite image (not shown), indicating that the cooling rate is larger in the model. At 03:28 UTC, the differences between model and satellite are relatively small (Figure 2). This is confirmed by statistics given in Table 2.

The mean satellite TSRAD at 03:28 UTC is a bit higher than the model one, as is indicated by a BIAS of 0.520 K. The standard deviation values are slightly above 2K, which is the maximum error associated to the TSRAD estimation process. The correlation coefficient is not very high (0.633), but its interpretation is not easy due to the complexity in the spatial distribution of the fields.

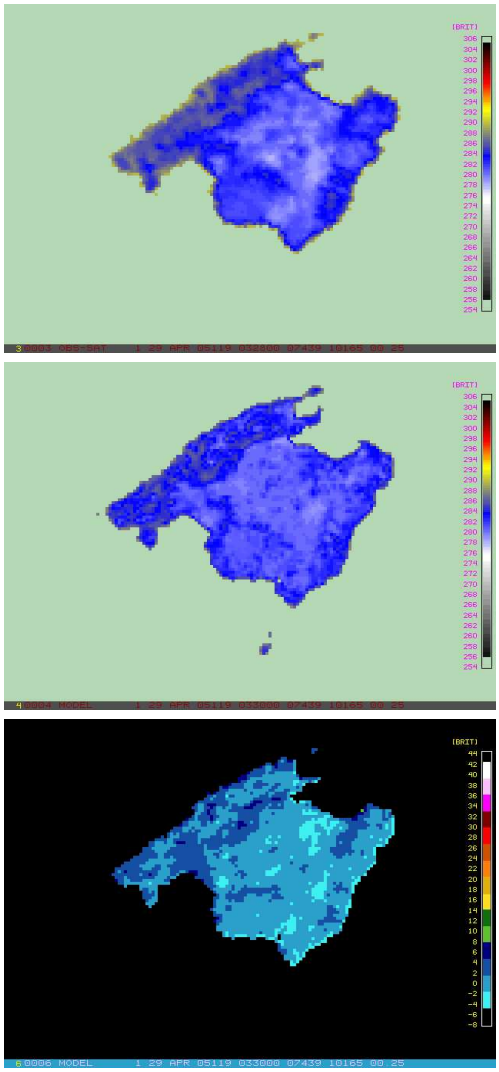

Figure 2: (a) Surface radiative temperature (TSRAD) of Majorca island calculated from the NOAA satellite image at 0328 UTC 29 April 2005; (b) same variable as (a) calculated from the model at 0330UTC; (c) differences between satellite and model TSRAD at 0330 UTC 29 April 2005

Without taking into account the model deficiencies, two different error sources were suspicious to be present in these images: a small displacement between model and satellite images due to an imprecision on the geometric adjustment of the satellite data, and an undesired inclusion of sea points into the verification data. In order to reduce the latter effect, a restriction in the temperature value over which the points are not verified was fixed in 287.55 K, to ensure the sea points would not be

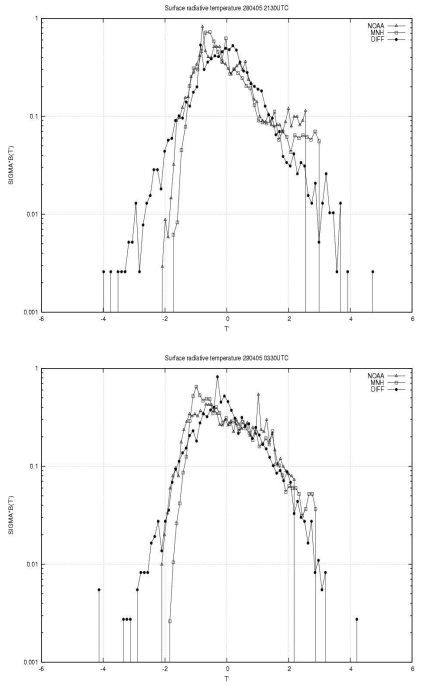

Figure 3: Normalized TSRAD PDFs at (a) 2130 UTC 28 April 2005 and (b) 0330 UTC 29 April 2005. Vertical axis has been multiplied by σ_T, and horizontal axis has been normalized to $T' = (T - \overline{T})/\sigma_T$. A log scale is chosen for the y-axis, which allow a better inspection of the PDFs tails.

included in verification. In addition, since it was detected a small displacement between images after the satellite one was geometrically adjusted, a program which moves the model image over the satellite one and searches for the best correlation between them was applied. Once this program was run, a 1km model image displacement was performed, which improved slightly the correlation coefficient to a value very close to 0.7.

At 21:30 UTC case, the BIAS is larger and the correlation coefficient smaller than for 03:30 UTC. The satellite is,in average, more than 1K warmer than the model, which is not a very large error. However the correlation coefficient, is quite low (0.361), showing the dissagreement between satellite and model spatial distribution of temperature. An improvement of the statistics can be achieved for this image if both the model and the satellite data are compared at a 4km resolution, meaning that the large structures are well captured, whereas the small scale ones are missed.

The probability density functions (PDFs) are used as a tool to interpret the two-dimensional surface radiative temperature field. $B(T)$ will be the probability of finding T between T and $T \pm \Delta T$, where ΔT is the bin or interval size (0.2 K here). The $B(T)$ probability function is usually normalized to allow for a better comparison of different PDFs (Figure 3). In Table 3 the values of the statistical parameters computed from the PDFs of the surface temperature fields out of the model, the satellite and the difference of both fields are given. The PDFs are not gaussian (which would give zero skewness and a value of 3 for the kurtosis). This is understandable, since the distribution of tempeatures is largely conditioned by the orography, which is no gaussian either. Nevertheless, the departure from the gaussianity is not very large, with the model having the maximum frequency slightly biased to the cold fluctuations.The majority of the fluctuations, both in the satellite and the model, are of less than 2 K from the mean value, and the model cold fluctuations are smaller than those from the satellite.

b. Verification of the temporal evolution using MSG-1 data

The infrared MSG images are used (one every 30') to study the temporal evolution of the estimated surface temperature field. The resolution is of 5 km at nadir. The comparison can be made to the model evolution and to the available data from the AWS (one record every 10 minutes). Four different AWS have been selected to make the comparison: two of them (Airport and Palma) near the sea, one of them (Lluc) inside a small valley placed at the northern mountain range, and the last one (Porreres) at a basin in the central part of the island. Plotted MSG data represent infrared channel 9 (10.8 μm) radiative temperature and they cannot be compared to the absolute Meso-NH TSRAD values, but to the Meso-NH TSRAD evolution. A better estimation of the real values is given by the NOAA images.

Two nearby stations in the Palma bay at the SW, show quite different results (Figs 4a and 4b) due to orographic features of the areas where they are placed. For the Airport, the model is about 3 k colder than the satellites during most of the night, whereas the 1.5 m temperature is well captured compared to the AWS. In this case the pixels

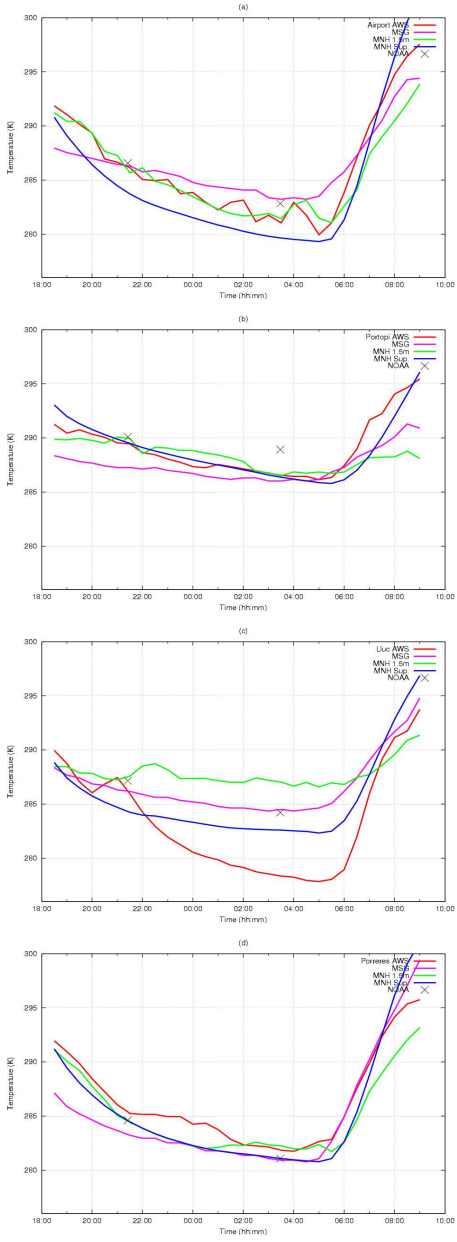

Figure 4: Time series of Meso-NH 1.5 m temperature and TSRAD outputs, MSG-1 channel 9 surface radiative temperature, and AWS 1.5 m temperature observations for the period between 1800 UTC 28 April 2005 and 0900 UTC 29 April 2005. Crosses are the TSRAD values from the NOAA images

from both satellite images contain a sea contribution, because the Airport is located just 3 kilometers far away the coast line, hence real temperature is smoothed. However, the model sees this area only as "land" pixel, explaining the better correspondance with the AWS. For the Palma station, temperature is 5 K higher than that measured at the airport during the whole night, since the Airport is located on a terrain depression where cold air accumulates, while the Palma station is in a ventilated area very close to the sea. The modeled temperature tendency in Palma shows a weak nocturnal cooling, while both satellites plots are much smoother because there exists a big contribution of the sea.

An interesting behaviour is found at Lluc station (Figure 4c), where orography of the model is interpolated over a complex terrain. Neither the model nor the satellites are able to see the surface cooling, since Lluc is located inside a cold pool and surrounding places are warmer than it. On the contrary, the Porreres station (Figure 4d) is in an area of gentle orography, well captured by the model and without relevant inhomogeneities to be smoothed by the satellite. In this case both the tendency and the actual values of modeled TSRAD temperature agree with MSG and NOAA data respectively, indicating a good performance of the model.

4.2 Surface winds

The verification of the wind field is only possible in a direct manner using the AWS. As an example, the wind velocity field at 00:00 UTc is shown in figure 5a, a time when the katabatic flows are well developed. The data show wind speeds below 1 m/s in most of the inland stations, values that are near the threshold of measurement of the AWS. It must be said that, in general, the wind direction is very well captured (Fig 5b) except for stations located in areas not representative, such as near buildings. A very significant issue is that the model is not able to generate calm winds and slightly overestimates the wind speeds in the cold areas in the center of the basins and in the stations in the litlle basins in the mountains.

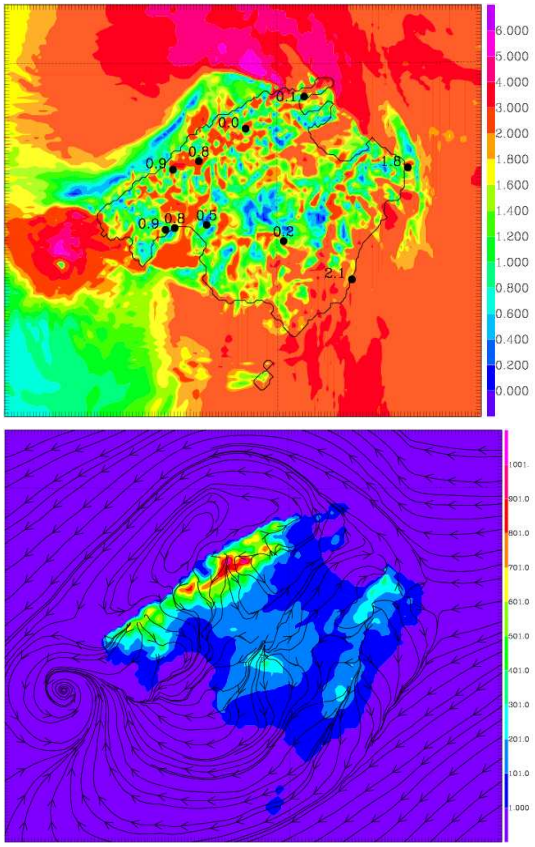

Figure 5: (a) Modeled and observed 10-m wind velocity at 0000 UTC; (b) 10-m stream lines at 0000 UTC

5 RE-INTERPRETATION OF THE SIMULATION

The evolution of the modelled night is discussed here, taking advantage of the available AWS and satellite information. The first hours of simulation are characterized by non-observed moderate winds at 10 m , but winds become weaker and more realistic as the night advances. Here the model suffers from an inadquate prescription of the initial and boundary conditions from the external analysis that is corrected afterwards. At 2130 UTC low temperatures are observed in most of inland, and are due to the absence of strong winds, which allow the land surface to cool quickly. At 0000 UTC the catabatic winds are completely stablished. At this time, modeled and observed winds are quite similar (Fig 5b), showing the good performance of the model to reproduce the orographic fluxes developed on complex terrain areas.

The non-normalized PDFs (Figure 6) allow to check some of the characteristics of the modelled field of surface temperature. At 21:28 UTC, the model is largely colder than the satellite, and the PDF is like shifted one degree to colder temperatures compared to the estimated PDF from the satellite. The cold temperatures are located in a narrow band, whereas the warm ones extend over a large band of values, surely conditioned by the local properties of the terrain. This bias is corrected at 03:30 UTC, when the colder model comes from the fact that the cold points are colder, but the distribution is very well captured. Looking at Figure 6b one would say that the model reproduces adequately the surface temperature field at 0300 UTC. The peak at the warm part of the PDFs corresponds to the points located in the mountain ranges.

The nocturnal cooling between the mentioned hours is plotted in Figure 6c. The model plot is centered in T=-3K, and the satellite one is centered in T=-4K, showing that the observed cooling is more intense than the modeled one, although both the model and the satellite agree that the coldest places of the island are those located at the lowest places and in the valleys, where cold air is stored during night. The nocturnal evolution of temperature at 2m is highly conditioned by the location in the island. Three different places can be differenced: (1) mountains, where nocturnal cooling is very strong at the valleys but not at elevated areas; (2) homogeneous orography regions, where the nocturnal cooling is also strong; and (3)coastal regions, where there is a high variability in wind direction but not in temperature, which is moduled by the sea. Results of the model for these regions show a reasonably agreement with observations, except for small valleys, that are not seen by the model.

From 0000 UTC until 0006 UTC the wind regime is near-stationary. Katabatic winds flow out of the island through the two largest basins (Palma and Alcúdia), coming mainly from the northern mountain range, but also from the smaller mountain range placed in the centre-south of the island. During the whole period, winds generated in the eastern range force the synoptic winds from east to surround the island.

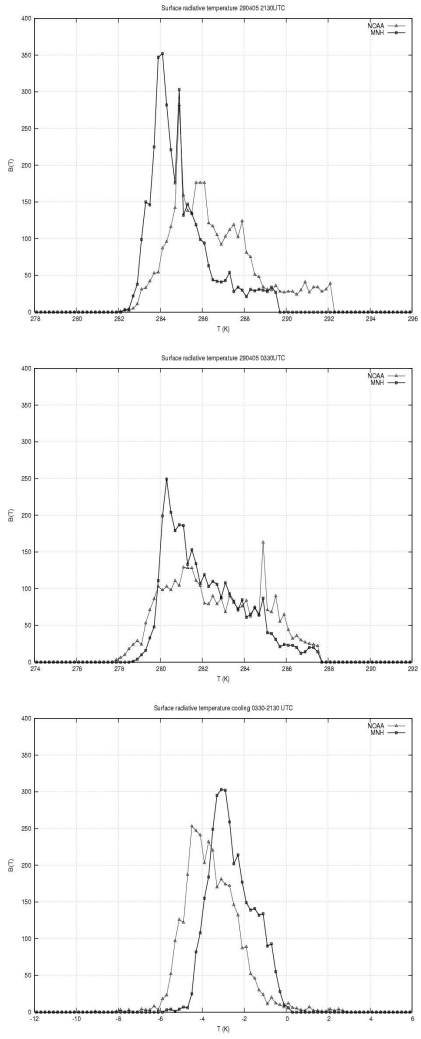

Figure 6: (a) TSRAD PDFs at 2130 UTC 28 April 2005 for model and satellite data; (b) same as (a) at 0330 UTC; (c) PDFs computed for the differences between 2130 UTC and 0330 UTC images (cooling)

6 SUMMARY

A clear-air mesoscale simulation under a slack pressure gradient has been studied using all the available observational information, which includes NOAA and MSG satellite imagery. The island generates is own system of local winds, and during nighttime the katabatic winds are ubiquitous on the mountain slopes, whereas the center of the basins cumulates cold air that is pushed to the sea by the basin outflows. The configuration of the wind structures is quasi-stationary during the second part of the night.

Due to the low number of available AWS, an effort has been made to use available information from satellite imagery. The estimate surface temperature from the NOAA and the MSG satellites is used as a 2D source of information. The direct comparison of the interpolated fields allows to check if the relevant structures are well captured, as well as the magnitude of the biases. It is found that these biases are of the same order as the error of the estimation method. The distribution of the fluctuations with respect to the average values is made by comparing the satellite and the model PDFs. In the second part of the night the correspondence is very good.

Two major limitations have appeared from this study: the smoothing of the orography by the model and the satellite, that makes the comparison to stations in singular areas useless, and the comparison with the satellite in areas where the pixel has contributions of the sea. Nevertheless, the method proves to be worth using, and gives confidence in the use of the Meso-NH model to perform clear-air mesoscale simulations under slack pressure gradients.

7 ACKNOWLEDGEMENTS

We acknowledge the European Center for Medium Range Weather Forecasts (ECMWF) for the access to its computing facilities, the Centre National de Recherches Météorologiques (Toulouse, France) for their support in the use of the Meso-NH model, and the Grup de Teledetecció of the Universitat de València for their support with the NOAA images treatment. We thank Daniel Martínez (UIB) for fruitful advice regarding satellite images, Maria Antònia Jiménez (UIB) for help regarding the PDFs construction and interpretation, and Lluís Fita (UIB) for invaluable help with some figures of this paper. The present study has been realized in the frame of the REN2003-09435 research project from Ministerio de Educación y Ciencia of the Spanish Government.

References

Bromwich, D.H. (1989). Satellite analyses of antarctic katabatic wind behavior. *Bulletin American Meteorological Society* **70**, 738–748.

Bromwich, D.H., Cassano, J.J., Klein, T., Heinemann, G., Hines, K.M., Steffen, K., and Box, J.E. (2001). Mesoscale modeling of katabatic winds over Greenland with the Polar MM5. *Monthly Weather Review* **129**, 2290–2309.

Chaboreau, J.-P., Cammas, J.-P., Mascart, P., Pinty, J.-P., Claud, C., Roca, R., and J.-J. Morcrette. (2000). Evaluation of a cloud system lifecycle simulated by Meso-NH during FASTEX using METEOSAT radiances and TOVS-31 cloud retrievals. *Quarterly Journal of the Royal Meteorological Society* **126**, 1735–1750.

Chu, C.R., Parlange, M.B., Katul, G.G., and Albertson, J.D. (1996). Probability density functions of turbulent velocity and temperature in the atmospheric surface layer. *Water Resources Research* **32**, 1681–1688.

Coll, C., Casellles, V., Sobrino, J.A., and Valor, E. (1994). On the atmospheric dependence of the split-window equation for land surface temperature. *International Journal of Remote Sensing* **15**, 105–122.

Coll, C., and Casellles, V. (1997). A split-window algorithm for land surface temperature from advanced very high resolution radiometer data: Validation and algorithm comparison. *Journal of Geophysical Research* **102**, 697–713.

Dash, P., Göttsche, F.-M., and Olesen, F.-S. (2002). Potential of MSG for surface temperature and emissivity estimation: considerations for real-time applications. *International Journal of Remote Sensing* **23**, 4511–4518.

Di, L., and Runquist, D.C. (1994). A one step algorithm for correction and calibration of AVHRR level 1b data. *Photogrammetric Engineering and Remote Sensing* **60**, 165–171.

Jiménez, M.A., and Cuxart, J. (2005). Study of the probability density functions from a large-eddy simulation for a stably stratified boundary layer. *Boundary-Layer Meteorology* (Published online).

Lafore, J.P., Stein, J., Asencio, N., Bougeault, P., Ducrocq, V., Duron, J., Fisher, C., Héreil, P., Mascart, P., Masson, V., Pinty, J.P., Redelsperger, J.-L., Richard, E. and Vilà-Guerau de Arellano, J. (1998). The Meso-NH atmospheric simulation system. Part I: Adiabatic formulation and control simulation. *Ann. Geophys.*, **16**, 90-109.

Martínez, D., Cuxart, J., and Jiménez, M.A. (2006). A case study of slope wind on the Majorca island. *Proc. 17th Symposium on Boundary Layers and Turbulence.* 22-25 May, San Diego, CA.

Prabha, T.V., Venkatesan, R., Sitaraman, V. (1999). Simulation of meteorological fields over a land-water-land terrain and comparison with observations. *Boundary-Layer Meteorology* **91**, 227–257.

Prata, A.J., Caselles, V., Coll, C., Sobrino, J.A., and Ottlé, C. (1995). Thermal remote sensing of land surface temperature from satellites: Current status and future prospects. *Remote sensing of Environment* **12**, 175–224.

Sobrino, J. A., Li, Z-L., Stoll, M. P., and Becker, F. (1996). Multi-channel amd multi-angle algorithms for estimating sea and land surface temperature with ATSR data. *International Journal of Remote Sensing* **17**, 2089–2114.

Soriano, C., Fernández, A., and Martin-Vide, J. (2005). Objective synoptic classification combined with high resolution meteorological models for wind mesoscale studies. *Meteorology and Atmospheric Physics* **91**, 165–181.

Stull, R.B. (1988). An introduction to boundary layer meteorology, Dordrecht. *Kluwer Academic Publishers*, 665 pp.

Station	AWS height(m)	MNH height(m)	Difference AWS-MNH(m)
Lluc	490	544	-54
Valldemossa	410	557	-147
Calvià	60	28	32
Portopí	3	5	-2
Serra Alfàbia	1030	769	261
Aeroport	4	10	-6
Porreres	120	124	-4
Far Portocolom	17	2	15
Far Capdepera	66	2	64
Port Pollença	2	37	-35

Table 1: Comparison between the AWS heights and their modeled values

Time	MEAN_OBS(K)	MEAN_MOD(K)	STD_OBS(K)	STD_MOD(K)	BIAS	R
2130 UTC	286.051	284.914	1.762	1.727	1.136	0.328
2130_d UTC	286.051	284.627	1.762	1.242	1.423	0.361
0330 UTC	282.609	282.179	2.239	2.219	0.430	0.585
0330_d UTC	282.609	281.975	2.239	1.806	0.634	0.691
COOLING	-3.745	-2.746	1.109	0.971	-0.999	0.263
COOLING_d	-3.645	-2.752	1.155	0.966	-0.892	0.474

Table 2: Statistics computed for NOAA and Meso-NH TSRAD images, where OBS and MOD means respectively observed and modeled. The d index means that model image has been displaced

Time	S_OBS	S_MOD	K_OBS	K_MOD
2130 UTC	0.69683	1.12925	2.72706	3.59825
0330 UTC	0.22250	0.77933	1.99825	2.81221
COOLING	0.89439	0.46929	5.44188	2.75542

Table 3: Kurtosis and skewness values computed for the PDFs of the TSRAD images, where OBS and MOD means respectively observed and modeled.